Automated structure-based learning to model co-operativity and protein-DNA interactions in *cis*-regulatory modules

Fornes O[1], Meseguer A[2], Aguirre-Plans J[2], Gohl, P[2], Mireia-Bota, P[2], Molina-Fernández R[2], Bonet J[2,3], Chinchilla, A[4], Pegenaute, F[4], Gallego, O[4], Fernandez-Fuentes,N[5], Oliva B[2]*

1 Centre for Molecular Medicine and Therapeutics, BC Children's Hospital Research Institute, Department of Medical Genetics, University of British Columbia, Vancouver, BC V5Z 4H4, Canada

2 Structural Bioinformatics Lab (GRIB-IMIM), Department of Medicine and Life Sciences, Universitat Pompeu Fabra, Barcelona 08005, Catalonia, Spain

3 Laboratory of Protein Design & Immunoengineering, School of Engineering, Ecole Polytechnique Federale de Lausanne, Lausanne 1015, Vaud, Switzerland

4 Live-Cell Structural Biology. Department of Medicine and Life Sciences, Universitat Pompeu Fabra, Barcelona 08005, Catalonia, Spain

5 Institute of Biological, Environmental and Rural Science, Aberystwyth University, SY23 3DA Aberystwyth, UK.

*To whom correspondence should be addressed: baldo.oliva@upf.edu

ABSTRACT

Transcription factor (TF) binding is a key component of genomic regulation. There are numerous high-throughput experimental methods to characterize TF-DNA binding specificities. Their application, however, is both laborious and expensive, which makes profiling all TFs challenging. For instance, the binding preferences of ~25% human TFs remain unknown; they neither have been determined experimentally nor inferred computationally. Here, we introduce a structure-based learning approach to predict the binding preferences of TFs and a web server to automatically model higher-order TF regulatory complexes (ModCRE). Our approach uses high-throughput TF binding data, such as from protein binding microarrays, to address the protein-DNA structure scarcity problem for learning the binding preferences of TFs. We show the conditional advantage of using our

approach over the state-of-art nearest-neighbor method for predicting TF binding sites. We improve prediction accuracy when using an enrichment selection system that uses many neighbors or structure-models. Starting from a TF sequence or structure, ModCRE predicts its binding preferences in the form of motifs. The predicted motifs are then used to scan a DNA sequence for occurrences, and the best matches are either profiled with a binding score or collected for their subsequent modeling into a higher-order regulatory complex with DNA. Co-operativity is modelled by: i) the co-localization of TFs; and ii) the structural modeling of protein-protein interactions between TFs and with co-factors. As case examples, we apply our approach to automatically model the interferon-β enhanceosome and the pioneering complex of OCT4, SOX2 and SOX11 with a nucleosome, which are compared with the experimentally known structures.

KEYWORDS

cis-regulatory modules, transcription factors co-operativity, structure-modeling of enhancers' complexes, models of pioneering transcription factors, structure-based learning.

Transcriptional regulatory elements in complex genomes are key players of the genome during development, cell and tissue homeostasis, responses to external stimuli, and disease[1]. Unravelling the mechanisms that regulate gene expression has become consequently one of the major challenges in biology. With this objective the increase in the scale of experimental data, across multiple data types, has provided a plethora of activating regulatory elements of the genome[2]. Classical definitions of activating regulatory elements are focused in two classes: promoters (where transcription is initiated) and enhancers (elements that amplify such transcription initiation in cis, i.e. located within less than 1M bases distance of the initiation). However, this distinction is becoming increasingly unclear, suggesting an updated model based on DNA accessibility of binding sites and enhancer/promoter potential [1]. The sequence preferences of transcription factors (TFs) for these binding sites can be assessed by a wide variety of experimental techniques, both in vitro (such as SELEX[3, 4], SMiLE-SEQ [5], protein-binding microarrays (PBM)[6-8] and MPRA[9, 10]) and in vivo (such as bacterial and yeast one hybrid assays[11, 12], ChIP-Seq[13] and other High-Throughput techniques[14, 15]). Recent models show similar potential of enhancers and promoters to promote the transcription machinery. Andersson et al.[1] have pointed towards the TF and RNA polymerase II-centric cooperative model, in which regulatory elements work together to increase or maintain the local concentrations of transcription factors (TFs), RNA polymerase II (RNAPII), and other co-factors, thereby increasing the probability to target gene transcription start sites.

Besides, it appears that very few proteins in human occupy most of their motif matches under physiological conditions[16], which highlights the importance of the balance between the co-operativity of TFs and their strength upon binding. Co-operative recognition of DNA by multiple TFs defines unique genomic positions on the genome and confers a systemic stability of regulation. Co-operative binding is most easily understood when it is mediated by protein-protein interactions that confer additional stability when two (or more) interacting proteins bind DNA[16]. Most eukaryotic TFs recruit cofactors as ‘‘coactivators’’ or ‘‘corepressors’’ forming large protein complexes to regulate transcription[17]. They commonly contain domains involved in chromatin binding, nucleosome remodelling, and/or covalent modification of histones or other proteins[16]. In the absence of direct protein–protein contacts between TFs, co-operativity can be mediated through DNA. Using CAP-SELEX[18] Jolma et al.[19] unveiled *in vitro* the co-operation of pairs of TFs through protein-protein and protein-DNA interactions. However, experimental protocols are both laborious and difficult to apply, and consequently most high-throughput efforts have been focused on few organisms.

Here, we have developed a structure-based learning approach to predict TF binding features and model the regulatory complex(es) in cis-regulatory modules (i.e. enhancers and promoters). Our objective is to characterize the role of structural elements, taking advantage of the recent developments on protein structure prediction (i.e. AlphaFold[20]) to reinforce both its modelling and prediction. Our approach integrates the experimental knowledge of structures of TF-DNA complexes and the large amount of high-throughput TF-DNA interactions to develop statistical knowledge-based potentials with which scoring the binding capability of TFs in cis-regulatory elements. We have developed a server to characterize and model the binding specificity of a TF sequence or its structure. The server can produce automatically structural models of TF-DNA interactions and their complexes with co-factors. The approach is applied on the examples of interferon-β enhanceosome[21] and the recent complex of “pioneer factors” Sox11/Sox2 and Oct4 with the nucleosome[22]. The model of interferon-β enhanceosome highlights the co-operativity of TFs with a more complete view of domain-domain interactions that were missed in the experimental structures. The model of the pioneering regulatory complex locates Oct4, which is missed in the experimental structure, suggesting a potential role for nucleosome opening.

Results

A structure-based learning approach to score TF-DNA interactions.

Many scoring methods have been proposed to assess the quality of protein fold models[23-25] and protein-protein interactions[26, 27]. One of the most common approaches are the knowledge-based potentials, also known as statistical

potentials[28-32]. In previous works we developed a set of potentials[33] to analyse protein structures and their interactions[34-36]. Ours is a structure-based learning approach that considers the frequency of contacts between pairs of residues and it includes their structural environment, such as solvent accessibility and type of secondary structure, to evaluate the interaction between proteins and nucleic-acids. The learning models are optimized by grid searching to get the best parameters of each TF family. However, a critical problem of this approach is the scarcity of known structures and in particular the scarcity of structures of protein-protein and protein-DNA interactions. We developed a method[37] for the TF family of C2H2 zinc-fingers (C2H2-ZF) that incorporated the interactions from systematic yeast-one-hybrid (Y1H) experiments[38]. Here, we have integrated the interactions derived with protein-binding microarray (PBM) experiments for several TF families using the dataset of CisBP[39, 40]. The space of contacts increases its coverage thanks to these experiments (see Figure 1). Details of the distribution of contacts are shown in heatmaps in the supplementary material (in http://aleph.upf.edu/modcre/##faq). Often the integration of experimental data from PBM increases the coverage of types of contacts and their number in several interval distances. For example, for AP2 and Homeodomain families, the use of PBM data substantially increases the number of contacts, while for the bHLH family the increase is more subtle (see Figure 1).

How well do we predict the binding preferences of TFs?.

We propose two tests to validate the predictive power of our approach: 1) evaluate the capacity to classify DNA 8-mers as bound/unbound for all TFs of the PBM experiments and specifically for the TFs of each family; and 2) evaluate the capacity to predict the DNA binding motifs of the TFs in the JASPAR dataset[41](which are described by means of position weight matrices, i.e. PWM), analyzing the results by TF families.

First, we tested the structure-based potential model (i.e. named in short $ZES3DC_{dd}$ in methods and supplementary material) on each TF to discern positive from negative 8-mers as described in the PBM experiments of the CisBP database (version 2.0) [40]. We avoided redundancies within the TFs of each family by filtering out all other TFs with more than 70% identical residues (i.e. the alignment of any pair of TF sequences of the same family has less than 70% identical residues). We scored the interaction of each TF with all their positive and negative 8-mers by modelling the TF-DNA complexes. We obtained precision-recall curves and calculated the area under the curve (AUPRC) to compare TF families and the features characterizing the structure-based learned potential (Figure 2). Interestingly some features were better than others depending on the family. Consequently, we designed a grid-search protocol to optimize the best features for each family of TFs to predict their PWMs (see methods). Second, we used these optimized parameters to predict the motifs of all TFs in JASPAR dataset[41] which structure could be modelled. Because many models of a TF can be obtained with different templates (i.e. the known structure of a close homolog interacting with a doble-strand DNA

helix), we forced to obtain 100 models for each TF, using all its templates from PDB[42] and the ability of MODELLER[43] to generate more than one conformation. We used the version of JASPAR 2020 consisting of 1934 PWMs. After discarding TFs with more than one PWM to avoid misinterpretation of predictions, the final dataset contained 1210 TFs (i.e. approximately 62% of the original dataset). Hence, we predicted 100 PWMs per TF and compared them with the experimental motif from JASPAR using TOMTOM[44]. We obtained the *P-value* provided by TOMTOM from each comparison and transformed it into a measure of similarity (*similarity score*) defined as $-log_{10}(Pvalue)$. Figure 3 shows the results of the prediction for several families of TFs by plotting the average (in Figure 3A) and the best scores (in Figure 3B) out of 100 models of each TF. For most TFs (around 75%) we predicted at least one motif significantly similar to the experimental (Pvalue < 0.05). The averages of scores of similarity were above a threshold of quality (stablished at Pvalue <0.05) for most TFs of the AP2, Nuclear Receptor, T-box, WRKY and bHLH families. Interestingly, the success to predict the binding preference was independent of the amount of data or the size of the binding site.

We studied more deeply the prediction for 177 TFs that have motifs in JASPAR and in CisBP (as obtained with PBMs). These TFs have 295 motifs in CisBP and 213 in JASPAR, which is about 20% of the original data with representation for most TF families. Considering that some TFs have more than one motif in JASPAR and in CisBP, the total number of comparisons between motifs was 369. All families except for TCR/CxC had at least one TF for which one model produced a PWM like the experimental (in JASPAR and CisBP). Table 1 shows the predicted motifs of a selected set of TFs compared with the experimental ones from JASPAR and CisBP. In supplementary Table S2 is shown a summary of the predictions for these TFs. From Table S2, considering successful the prediction for a TF if more than 50% of the predicted PWMs are significatively like the experimental motif, we predicted right almost 48% TFs' motifs compared with JASPAR and 57% with CisBP. Then, if we consider successful the prediction for a TF if at least one of the predicted PWMs is significatively similar to the experimental motif, we predicted right 82% motifs compared with JASPAR and 89% with CisBP.

How good our approach is compared with the state-of-art (nearest-neighbor).

We compared the prediction of the PWM with the state-of-art based on sequence homology. This approach is also known as prediction by nearest-neighbor. The nearest neighbor approach consists on using the experimental PWM of the closest homolog of a TF[45]. The accuracy of such prediction depends on the degree of similarity between TFs: hypothetically, close homologs should have similar DNA binding domains and in consequence their PWMs should be similar too. As dataset, we used the TFs of CisBP that had been studied by PBMs. First, we compared their sequences using MMseq2[46]. Then, for each target sequence we grouped the other TFs of the dataset by sequence similarity with the target. Each group contains sequences with a maximum percentage of sequence identity with the target and the

groups range between 15% and 95% in bins with intervals of 10% (e.g. the group at 95% contains all closest homologs of a target TF which alignment produces 95% identical residues or less). The analysis of the prediction was performed grouping TFs by families and the results by bins of the same interval of sequence similarity. Notice that not for all TFs in the dataset it was possible to find relatives in all bins. For the nearest-neighbor approach, given a family and a bin, we used the PWM of the most similar TF in the bin (i.e. the motif of the TF which sequence aligns with the target with highest percentage of identity). For our structure-based approach, given a family and a bin, we used the same TFs tested in the nearest neighbor approach, for which we modelled 100 conformations (i.e. consequently predicting 100 motifs). Then, we tested the success of the prediction by ranking the results: we used TOMTOM[47] from the MEME suit[44] to compare the predicted PWM (or PWMs) with all the experimental motifs from CisBP, including the motif that corresponds to the target, and ranked them according to TOMTOM score. The rank of the actual motif of the target indicates the quality of the prediction. We scored and normalized the rank to fit between 0 and 100 (then the highest score is achieved with the best rank, see details in the legend of Figure 4 and further in supplementary material section). Notice that the prediction based on structural models has 100 times more solutions than the nearest neighbor approach. The prediction for all TFs is produced by the accumulation of results for all families in each bin (see Figure 4). For some families the structure-based predictions outperformed the nearest neighbor approach at bins around 50% of sequence identity (i.e. families such as Forkhead, Nuclear Receptor and SOX). However, for most families our predictions were worse than the nearest neighbor approach at bins with high percentage of identity and only outperformed it at very low identity percentages (i.e. around 15%, as for families C2H2 ZF, ETS and Homeodomain).

How to improve the prediction of binding preferences of TFs.

As observed in the structure-based prediction of motifs, we generated several PWMs for a target TF. This suggests a potential new approach to predict the motif of a TF that can also be applied in the nearest-neighbor approach. We propose to use the most often selected motif within the best rankings as the solution of our prediction. For the nearest-neighbor approach, instead of selecting the PWM of the closest homolog, we consider all the motifs of TFs with sufficiently similar sequence to the target. Thus, a collection of motifs is used as in the structure-based approach. We name the approach “rank-enrichment prediction”. As in the previous ranking of motifs of the dataset (which includes the actual motif of the TF target), we rank by the score of TOMTOM the motifs of the database for all the predicted PWMs of the target. We remove all non-significantly aligned PWMs and select a limited number of potential solutions. The number of potential solutions affects the quality of the prediction: if we use too many the success is not significant, or in other words, it can be achieved by random (see more details in the supplementary material). In the selected set, some motifs may have been included several times. Then, we calculate the enrichment of a motif as the ratio of the number of times it appears in the selection. The final

prediction corresponds to the motif with highest enrichment (i.e. the motif that was more often selected, either among homologs of the target in the nearest-neighbor approach, or among modelled conformations in the structure-based approach). Finally, to evaluate the quality of the predicted motif, we compare it with the motifs of the database and calculate the ranking of the score of the actual motif of the target. The ranking is scored and normalized as before, and the distribution is plotted for several bins of sequence-similarity. We must note that now a single solution is proposed for each TF in both approaches, nearest-neighbor and structure-based with ModCRE. Figure 5 shows the distribution of the normalized ranking on the application of rank-enrichment prediction with both approaches. The rank-enrichment approach increased the accuracy of the predictions of both methods. Furthermore, as observed previously, the structure-based approach often achieves better rankings than nearest-neighbor at low percentages of similarity.

Applying a majority vote to predict the binding sites of TFs

In practice, there is no access to the real motif(s) of a TF and consequently the rank-enrichment approach cannot be applied straight-forward. However, the approach indicates that the best prediction is produced by a majority of similar motifs out of a collection of predicted PWMs. Therefore, a sensible approach to predict the binding site of a TF in a DNA sequence is: 1) to predict a set of PWMs (either by nearest-neighbor or with the structure-based approach, and more specifically the last one if the homologs of the target are not sufficiently similar); 2) scan the DNA sequence with all predicted motifs using FIMO[48]; and 3) select the fragment matched by the majority of motifs with a significant score (i.e. Pvalue<0.05).

To analyze the binding sites of a DNA sequence, we have developed a web server that predicts the PWM of a TF based on its structure or by modelling several conformations with its sequence. Then, the DNA sequence can be scanned with the PWMs and either the accumulation of matches can be profiled (i.e. using a score for the prediction of binding), or a selection of matches can be collected to build the structure of a cooperative binding (i.e. considering the formation of a potential complex of transcription). To facilitate the scanning of a large DNA sequence and the construction of a structural model of cooperative binding, we have included the PWMs of three datasets associated with TF structures. Two datasets are defined with the experimental motifs from JASPAR and CisBP. In each of these sets a motif is associated with the sequence of a TF. Therefore, we have modelled the potential conformations of each one of these TFs and selected the model with the PWM most similar to the experimental motif. Then, a target DNA sequence is scanned with FIMO using the motifs of the corresponding database and the associated models can be selected in ModCRE. Similarly, a third database is obtained using the structures of TFs complexed with a DNA double strand: we use BLAST[49] and HMMER[50] to obtain the sequences of potential homologs in UniProt and TrEMBL[51] that align (without gaps in the binding interface) with the sequences of these TFs. A motif is predicted for any of these sequences using the alignment and the template

structure. Consequently, we can scan the DNA with any of the sequences of specific species (see further details in supplementary material). Additionally, specific TF sequences can be uploaded to predict their motifs and scan the DNA.

Integrative modelling of transcription factors and co-factors of cis-regulatory modules.

To complete the modelling, co-factors can be included in the network of interactions when the species selected are human or mouse. Interactions between TFs and transcription co-factors (TcoFs) are retrieved from the TcoF-DB database[52]. After selecting a set of protein-protein and protein-DNA interactions, these can be modeled using a homology modeling pipeline[26, 35]. Then, ModCRE models the structure of DNA in a specific conformation (which by default is in B conformation), and for very long DNA sequences the server splits the sequence in fragments of 250 base-pairs (with an overlap of 50bp to be able to assemble them later). Models with clashes between proteins are removed and only acceptable combinations of each fragment are selected to construct a model. Next, the structures are optimized by several steps of conjugate gradient and short annealing dynamic simulations with MODELLER. Finally, distance restraints are extracted from the models of protein-protein interactions and TF-DNA interactions, and we use the package IMP[53] to integrate them in a model of DNA with all TFs and TcoFs (see more details in supplementary material).

Example: the interferon-beta (IFN-β) enhanceosome

We have used the server to automate the modelling of the interferon-beta (IFN-β) enhanceosome, an ensemble of TFs and Cis-regulatory elements that cooperate in the enhancer of the IFN-β gene[21, 54]. The TFs joining at the IFN-β enhanceosome are ATF-2, c-Jun, IRF-3, IRF-7, and NFKβ-1 (subunits p105 and p65). We have used a sequence of 250bp containing the region of the enhanceosome and the database of human TFs, using their predicted PWMs based on their modelled structures, to predict and model the co-operative complex. These PWMs are used to scan the DNA sequence with FIMO. In supplementary Figure S4 we select the bindings of the specific TFs (i.e. ATF-2, c-Jun, IRF-3, IRF-7, and NFKβ-1) that are significative (P-values < $5.0e^{-4}$). Hence, we are able to recreate a structural model similar to the model provided by Panne[21, 54] based on experimental data. On the binding sites predicted for NFKβ-1 (subunits p105 and p65) the automated approach produces a homodimer of NFKβ-1 with two subunits p105 instead of a heterodimer with RelA (subunit p65). Not all the binding regions of IRF-3 are detected exactly, but some other regions are predicted instead. Besides, the IRF-7 binding site from Panne's model is occupied by IRF-3. The analysis highlights the accumulation of TFs in a short section of the DNA and brings a potential explanation for the formation of the transcription complex by gathering TFs (Figure 6).

Example: TF-DNA interactions on top of the nucleosome.

An interesting case of co-operation between TFs are the "pioneer factors" (the first to engage target sites in chromatin culminating in transcription by displacing nucleosomes[55]), or TFs that can bind on top of the nucleosome complex (as detected by NCAP–SELEX[56]). A structural view of this complex has shed light on the characteristics of the TF-DNA interaction and its effect upon the conformation of the nucleosome[22]. The server has also the possibility to produce a bent conformation such as the nucleosome that includes histones to form the complex (IMP is not applied because the structure of DNA is already defined). We have used the automated modelling of a nucleosome in complex with Sox2, Sox11 and Oct4 from the study of Dodonova et al. [22] to analyze these "pioneer factors". Interestingly, using the PWM predicted using ModCRE, Sox2 and Sox11 find two very significant binding regions (P-value <$1.0e^{-4}$, around 58bp and 85bp positions) that are hampered by histones, while 3 sites are found with less significance (P-value < $1.0e^{-3}$) but accessible to Sox11/Sox2 and Oct4 (Sox11 and Sox2 share the same binding site preferences). However, Sox2 is missing in the predicted complex and the models of Sox11 and Oct4 clash with the DNA, implying the need of a posterior distortion to produce the complex (Figure 7). For Oct4 the model recreates the binding with both domains, but we must notice that with only one domain the binding is possible without producing clashes in the nucleosome second turn of DNA (in 98-112bps).

Discussion

TF-binding specificities are foremost to understand gene regulation. Still, the binding preferences for many eukaryotic TFs are unknown or very complex *in vivo*[7, 57]. In this regard, computational tools are a challenging complement to experimental methods. In this work we have developed a structure-based approach to predict specific binding motifs of TFs, to identify cis-regulatory elements and to automatically model the structure of the transcription complex entailing the regulation. The approach has been implemented in a server for the scientific community named ModCRE. The main limitation of our approach is that it can only be applied to TFs for which we have a structure of the interaction with DNA. The scarcity of these experimental structures also affects the number of templates to be used by homology modeling. Supplementary figure S5 shows the number of TFs from UniProt database where we can apply ModCRE using comparative modelling. This proves that we can apply ModCRE to most families of TFs, and in combination with JASPAR database our approach can be applied to 88.7% of the TF sequences. Besides, thanks to the recent advent of AlphaFold2 [20, 58] the structure of almost all TFs can be predicted, and remarkably the DNA binding motif, that often contains a large percentage of regular secondary structures, can be build. Then, the structure of any TF-DNA complex can be modelled either by docking or by superposition with other members of the TF family. As a tailored example we have studied the human motif of the

CCAAT/enhancer-binding protein alpha (*C/EBPα.*). The human protein has not been crystallized, but the DNA binding motif of rat is 100% identical and the structure of the dimer is available in PDB with code 1NWQ [59]. Then, we downloaded the AlphaFold structure of *C/EBPα.* from human (AF-P49715-F1 from UniProt) and select only the DNA binding domain (α-helix residues 284-344). We superposed this domain on each chain of the structure of the heterodimer of ATF-2 and c-Jun (PDB code 1T2K [60]) to get the dimer complex of *C/EBPα.* with DNA. We used both structures to predict the PWM with ModCRE, one by submitting the sequence and getting the motif with 1NWQ as template, and the other by submitting the structure. This example shows almost identical motifs (see supplementary figure S6).

By incorporating the structural variability and flexibility of a TF we have designed an improvement of the prediction of its binding-sites based on the largest preference of motifs, each motif generated with one conformation. Thus, by scanning with several predicted motifs of a TF, the majority of regions detected and predicted to bind will hit around the right location of the binding site. Using a collection of motifs derived from different models of a TF is in consonance with the idea that TFs can interact with the DNA adopting different conformations[7]. Homology modelling is very convenient when several templates are available because it generates a collection of models of a TF, and similarly AlphaFold can be applied to obtain several conformations. ModCRE's modeling pipeline is also a valuable resource to study the conformations of large regulatory complexes. Structural models of TF-DNA interactions provide fundamental information to understand TF function and behavior. Our pipeline model complexes of TF-DNA interactions involving DNA bindings and protein-protein interactions between TFs and transcription co-factors. We hypothesize that the correct binding site is among the selection of sites where most conformations of TFs accumulate when considering the cooperation with other TFs and co-factors. This may be a promising strategy helping to overcome the number of false positives found when scanning a DNA sequence with a single PWM[7, 57] or at least to narrow the predictions and simultaneously comprehend the cooperativity between transcription factors and co-factors.

Methods

Software

We use DSSP (version CMBI 2006)[61] to obtain the secondary structure and surface accessibility; X3DNA (version 2.0)[62] to obtain DNA structures; *matcher* and *needle*, from the EMBOSS package (version 6.5.0)[63], to obtain local and global alignments, respectively; BLAST (version 2.2.22)[49] to obtain potential homologs of a protein sequence; MODELLER (version 9.9)[43] to model the structure of a protein by homology; CD-HIT to obtain a non-redundant set of sequences of TFs[64] and the programs FIMO[48] and TOMTOM of the MEME suite[44] to obtain the fragments of a DNA sequence that aligns with a Position-Weight Matrix (PWM) [65] and to compare two PWMs, respectively.

Databases

Atomic coordinates of protein complexes are retrieved from the PDB repository[66] and protein codes and sequences are extracted from UniProt[51]. We only selected the structures of PDB corresponding to TF-DNA interactions. Binding information of TFs was obtained from protein binding microarray (PBM) experiments in the Cis-BP database (version 2.00) [40, 67]. PBM experiments indicate the binding affinity between TFs and DNA 8-mers with the E-score value (between -0.50 and 0.50). DNA 8-mers of a TF with E-scores above 0.45 correspond to high affinity interactions (also named positive), while DNA 8-mers with E-scores below 0.37 are considered non-bound (or negative); the rest of E-scores are discarded for statistic analyses.

Interface of protein-DNA structures

We defined the contacts between TF and DNA using three residues: one amino acid and two contiguous nucleotides of the same strand. The distance of a contact is the distance between the Cβ atom of the amino acid residue and the average position of the atoms of the nitrogen-bases of the two nucleotides and their complementary pairs in the opposite strand[28]. Additional features are considered for a contact, such as the secondary structure and solvent accessibility of the amino-acid or the DNA closest groove (major or minor) of the two nucleotides.

Knowledge-based potentials

We used the definition of statistical potentials described by Feliu et al.[68] and Fornes et al.[28]. These were calculated with the distribution of contacts at less than 30 Å, using an interval criterion or a distance threshold. We use positive DNA 8-mers from PBMs to extend the number of contacts. We transformed the statistical potentials into Z-scores to identify the contacts with best scores (best distance and best contact residues: i.e. the amino acid and the two nucleotides).

Structural modeling of TF-DNA complexes

Several structural models of a TF-DNA complex were obtained using all its available templates from PDB. First we used BLAST to find the homologs with known structure (template), then the sequence of the query was aligned with the sequences of the templates using MATCHER from the EMBOSS package[63] and a model was built with each template using MODELLER[43]. The modeling of the DNA was obtained with the X3DNA package[62] preserving the DNA conformation from the template. This approach required that all the templates used for TF-DNA modeling contained both a TF and a double stranded DNA molecule.

Construction of PWMs using TF-DNA structural models

We used the Z-scores of statistical potentials to obtain the PWM. We selected for each TF family the features optimizing the PWM prediction (see further) and we used the Z-score of $ES3DC_{dd}$ ($ZES3DC_{dd}$) as defined in Meseguer et al. [37]. First, we obtained several models of a TF-DNA interaction using all possible templates. Second, for each model we scored all the potential DNA sequences of the binding site (i.e. 4^N sequences, with N the size of the binding site, or an alternative heuristic approach as explained in the supplementary). Third, we normalized the scores between 0 and 1 and we ranked the DNA sequences. Finally, for each model we selected the sequences with the top scores (this cut-off threshold was also optimized, taking values between 0.7 and 1 in intervals of 0.01). We used the alignment of these sequences to calculate a predicted PWM for each model.

Optimization of parameters by grid search.

The parameters to predict PWMs that needed to be optimized for each TF family are: 1) the definition of distances' distribution used to calculate statistical potentials: either by interval-bins (i.e. $x - 1 < d \leq x$) or a threshold (i.e. $d \leq x$); 2) the use of a theoretical approach to complete the space of contacts (i.e. using a Taylor's polynomial approach, see supplementary); 3) the dataset of structures used to calculate the potentials: using only the contacts from structures of PDB or adding those from experiments of PBMs; 4) using a general potential learned with all known TF-DNA structures or a specific potential calculated with the structures of the same family and fold; 5) the maximum distance to include the contacts of an interface (testing distances at 15 Å, 22 Å and 30 Å); and 6) the cut-off threshold to select top ranked DNA sequences used to calculate the PWM (see above). The function to be optimized was the accuracy to predict the PWM of each TF family (i.e. maximum accuracy). A predicted PWM was successful if the alignment with the experimental PWM taken from Cis-BP database was significant (this was calculated with TOMTOM). Then, we selected the parameters that maximized the accuracy of the TF family with the following conditions: 1) maximum number of significant good predictions according to TOMTOM score; 2) best TOMTOM scores when a similar

number of significant solutions were achieved; and 3) the lowest value of the threshold, when several similar solutions were obtained.

References

1. Andersson, R. & Sandelin, A. Determinants of enhancer and promoter activities of regulatory elements. *Nat Rev Genet* **21**, 71-87 (2020).
2. Consortium, E.P. et al. Expanded encyclopaedias of DNA elements in the human and mouse genomes. *Nature* **583**, 699-710 (2020).
3. Hallikas, O. & Taipale, J. High-throughput assay for determining specificity and affinity of protein-DNA binding interactions. *Nat Protoc* **1**, 215-222 (2006).
4. Roulet, E. et al. High-throughput SELEX SAGE method for quantitative modeling of transcription-factor binding sites. *Nat Biotechnol* **20**, 831-835 (2002).
5. Isakova, A. et al. SMiLE-seq identifies binding motifs of single and dimeric transcription factors. *Nat Methods* **14**, 316-322 (2017).
6. Berger, M.F. & Bulyk, M.L. Protein binding microarrays (PBMs) for rapid, high-throughput characterization of the sequence specificities of DNA binding proteins. *Methods Mol Biol* **338**, 245-260 (2006).
7. Badis, G. et al. Diversity and complexity in DNA recognition by transcription factors. *Science* **324**, 1720-1723 (2009).
8. Hume, M.A., Barrera, L.A., Gisselbrecht, S.S. & Bulyk, M.L. UniPROBE, update 2015: new tools and content for the online database of protein-binding microarray data on protein-DNA interactions. *Nucleic Acids Res* **43**, D117-122 (2015).
9. Patwardhan, R.P. et al. High-resolution analysis of DNA regulatory elements by synthetic saturation mutagenesis. *Nat Biotechnol* **27**, 1173-1175 (2009).
10. Melnikov, A. et al. Systematic dissection and optimization of inducible enhancers in human cells using a massively parallel reporter assay. *Nat Biotechnol* **30**, 271-277 (2012).
11. Meng, X. & Wolfe, S.A. Identifying DNA sequences recognized by a transcription factor using a bacterial one-hybrid system. *Nat Protoc* **1**, 30-45 (2006).
12. Deplancke, B., Dupuy, D., Vidal, M. & Walhout, A.J. A gateway-compatible yeast one-hybrid system. *Genome Res* **14**, 2093-2101 (2004).
13. Ambrosini, G., Dreos, R., Kumar, S. & Bucher, P. The ChIP-Seq tools and web server: a resource for analyzing ChIP-seq and other types of genomic data. *BMC Genomics* **17**, 938 (2016).
14. Blecher-Gonen, R. et al. High-throughput chromatin immunoprecipitation for genome-wide mapping of in vivo protein-DNA interactions and epigenomic states. *Nat Protoc* **8**, 539-554 (2013).
15. Umeyama, T. & Ito, T. DMS-Seq for In Vivo Genome-wide Mapping of Protein-DNA Interactions and Nucleosome Centers. *Cell Rep* **21**, 289-300 (2017).
16. Lambert, S.A. et al. The Human Transcription Factors. *Cell* **172**, 650-665 (2018).
17. Reiter, F., Wienerroither, S. & Stark, A. Combinatorial function of transcription factors and cofactors. *Curr Opin Genet Dev* **43**, 73-81 (2017).

18. Morgunova, E. & Taipale, J. Structural perspective of cooperative transcription factor binding. *Curr Opin Struct Biol* **47**, 1-8 (2017).
19. Jolma, A. et al. DNA-dependent formation of transcription factor pairs alters their binding specificity. *Nature* **527**, 384-388 (2015).
20. Jumper, J. et al. Highly accurate protein structure prediction with AlphaFold. *Nature* **596**, 583-589 (2021).
21. Panne, D. The enhanceosome. *Curr Opin Struct Biol* **18**, 236-242 (2008).
22. Dodonova, S.O., Zhu, F., Dienemann, C., Taipale, J. & Cramer, P. Nucleosome-bound SOX2 and SOX11 structures elucidate pioneer factor function. *Nature* **580**, 669-672 (2020).
23. Marti-Renom, M.A., Madhusudhan, M.S., Fiser, A., Rost, B. & Sali, A. Reliability of assessment of protein structure prediction methods. *Structure* **10**, 435-440 (2002).
24. Wiederstein, M. & Sippl, M.J. ProSA-web: interactive web service for the recognition of errors in three-dimensional structures of proteins. *Nucleic Acids Res* **35**, W407-410 (2007).
25. Studer, G. et al. QMEANDisCo-distance constraints applied on model quality estimation. *Bioinformatics* **36**, 2647 (2020).
26. Mirela-Bota, P. et al. Galaxy InteractoMIX: An Integrated Computational Platform for the Study of Protein-Protein Interaction Data. *J Mol Biol* (2020).
27. Moal, I.H., Moretti, R., Baker, D. & Fernandez-Recio, J. Scoring functions for protein-protein interactions. *Curr Opin Struct Biol* **23**, 862-867 (2013).
28. Fornes, O., Garcia-Garcia, J., Bonet, J. & Oliva, B. On the use of knowledge-based potentials for the evaluation of models of protein-protein, protein-DNA, and protein-RNA interactions. *Adv Protein Chem Struct Biol* **94**, 77-120 (2014).
29. Sippl, M.J. Knowledge-based potentials for proteins. *Curr Opin Struct Biol* **5**, 229-235 (1995).
30. Huang, S.Y. & Zou, X. An iterative knowledge-based scoring function for protein-protein recognition. *Proteins* **72**, 557-579 (2008).
31. Moretti, R. et al. Community-wide evaluation of methods for predicting the effect of mutations on protein-protein interactions. *Proteins* **81**, 1980-1987 (2013).
32. Dhawanjewar, A.S., Roy, A.A. & Madhusudhan, M.S. A knowledge-based scoring function to assess quaternary associations of proteins. *Bioinformatics* **36**, 3739-3748 (2020).
33. Aguirre-Plans, J. et al. SPServer: split-statistical potentials for the analysis of protein structures and protein-protein interactions. *BMC Bioinformatics* **22**, 4 (2021).
34. Segura, J., Marin-Lopez, M.A., Jones, P.F., Oliva, B. & Fernandez-Fuentes, N. VORFFIP-driven dock: V-D2OCK, a fast and accurate protein docking strategy. *PLoS One* **10**, e0118107 (2015).
35. Meseguer, A. et al. Using collections of structural models to predict changes of binding affinity caused by mutations in protein-protein interactions. *Protein Sci* **29**, 2112-2130 (2020).

36. Meseguer, A., Bota, P., Fernandez-Fuentes, N. & Oliva, B. Prediction of Protein-Protein Binding Affinities from Unbound Protein Structures. *Methods Mol Biol* **2385**, 335-351 (2022).
37. Meseguer, A. et al. On the prediction of DNA-binding preferences of C2H2-ZF domains using structural models: application on human CTCF. *NAR Genom Bioinform* **2**, lqaa046 (2020).
38. Persikov, A.V., Rowland, E.F., Oakes, B.L., Singh, M. & Noyes, M.B. Deep sequencing of large library selections allows computational discovery of diverse sets of zinc fingers that bind common targets. *Nucleic Acids Res* **42**, 1497-1508 (2014).
39. Weirauch, M.T. et al. Determination and inference of eukaryotic transcription factor sequence specificity. *Cell* **158**, 1431-1443 (2014).
40. Lambert, S.A. et al. Similarity regression predicts evolution of transcription factor sequence specificity. *Nat Genet* **51**, 981-989 (2019).
41. Fornes, O. et al. JASPAR 2020: update of the open-access database of transcription factor binding profiles. *Nucleic Acids Res* **48**, D87-D92 (2020).
42. Burley, S.K. et al. RCSB Protein Data Bank: Celebrating 50 years of the PDB with new tools for understanding and visualizing biological macromolecules in 3D. *Protein Sci* **31**, 187-208 (2022).
43. Webb, B. & Sali, A. Comparative Protein Structure Modeling Using MODELLER. *Curr Protoc Bioinformatics* **54**, 5 6 1-5 6 37 (2016).
44. Bailey, T.L., Johnson, J., Grant, C.E. & Noble, W.S. The MEME Suite. *Nucleic Acids Res* **43**, W39-49 (2015).
45. Fuxman Bass, J.I. et al. Transcription factor binding to Caenorhabditis elegans first introns reveals lack of redundancy with gene promoters. *Nucleic Acids Res* **42**, 153-162 (2014).
46. Steinegger, M. & Soding, J. MMseqs2 enables sensitive protein sequence searching for the analysis of massive data sets. *Nat Biotechnol* **35**, 1026-1028 (2017).
47. Gupta, S., Stamatoyannopoulos, J.A., Bailey, T.L. & Noble, W.S. Quantifying similarity between motifs. *Genome Biol* **8**, R24 (2007).
48. Grant, C.E., Bailey, T.L. & Noble, W.S. FIMO: scanning for occurrences of a given motif. *Bioinformatics* **27**, 1017-1018 (2011).
49. Altschul, S.F. et al. Gapped BLAST and PSI-BLAST: a new generation of protein database search programs. *Nucleic Acids Res* **25**, 3389-3402 (1997).
50. Potter, S.C. et al. HMMER web server: 2018 update. *Nucleic Acids Res* **46**, W200-W204 (2018).
51. UniProt, C. UniProt: the universal protein knowledgebase in 2021. *Nucleic Acids Res* **49**, D480-D489 (2021).
52. Schmeier, S., Alam, T., Essack, M. & Bajic, V.B. TcoF-DB v2: update of the database of human and mouse transcription co-factors and transcription factor interactions. *Nucleic Acids Res* **45**, D145-D150 (2017).
53. Hancock, M. et al. Integration of software tools for integrative modeling of biomolecular systems. *J Struct Biol*, 107841 (2022).
54. Panne, D., Maniatis, T. & Harrison, S.C. An atomic model of the interferon-beta enhanceosome. *Cell* **129**, 1111-1123 (2007).

55. Zaret, K.S. & Carroll, J.S. Pioneer transcription factors: establishing competence for gene expression. *Genes Dev* **25**, 2227-2241 (2011).
56. Zhu, F. et al. The interaction landscape between transcription factors and the nucleosome. *Nature* **562**, 76-81 (2018).
57. Medina-Rivera, A. et al. Theoretical and empirical quality assessment of transcription factor-binding motifs. *Nucleic Acids Res* **39**, 808-824 (2011).
58. Jumper, J. & Hassabis, D. Protein structure predictions to atomic accuracy with AlphaFold. *Nat Methods* **19**, 11-12 (2022).
59. Miller, M., Shuman, J.D., Sebastian, T., Dauter, Z. & Johnson, P.F. Structural basis for DNA recognition by the basic region leucine zipper transcription factor CCAAT/enhancer-binding protein alpha. *J Biol Chem* **278**, 15178-15184 (2003).
60. Panne, D., Maniatis, T. & Harrison, S.C. Crystal structure of ATF-2/c-Jun and IRF-3 bound to the interferon-beta enhancer. *EMBO J* **23**, 4384-4393 (2004).
61. Kabsch, W. & Sander, C. Dictionary of protein secondary structure: pattern recognition of hydrogen-bonded and geometrical features. *Biopolymers* **22**, 2577-2637 (1983).
62. Lu, X.J. & Olson, W.K. 3DNA: a software package for the analysis, rebuilding and visualization of three-dimensional nucleic acid structures. *Nucleic Acids Res* **31**, 5108-5121 (2003).
63. Rice, P., Longden, I. & Bleasby, A. EMBOSS: the European Molecular Biology Open Software Suite. *Trends Genet* **16**, 276-277 (2000).
64. Fu, L., Niu, B., Zhu, Z., Wu, S. & Li, W. CD-HIT: accelerated for clustering the next-generation sequencing data. *Bioinformatics* **28**, 3150-3152 (2012).
65. Wasserman, W.W. & Sandelin, A. Applied bioinformatics for the identification of regulatory elements. *Nat Rev Genet* **5**, 276-287 (2004).
66. Rose, P.W. et al. The RCSB protein data bank: integrative view of protein, gene and 3D structural information. *Nucleic Acids Res* **45**, D271-D281 (2017).
67. Weirauch, M.T. et al. Determination and inference of eukaryotic transcription factor sequence specificity. *Cell* **158**, 1431-1443 (2014).
68. Feliu, E., Aloy, P. & Oliva, B. On the analysis of protein-protein interactions via knowledge-based potentials for the prediction of protein-protein docking. *Protein Sci* (2011).
69. Escalante, C.R., Nistal-Villan, E., Shen, L., Garcia-Sastre, A. & Aggarwal, A.K. Structure of IRF-3 bound to the PRDIII-I regulatory element of the human interferon-beta enhancer. *Mol Cell* **26**, 703-716 (2007).

Figures

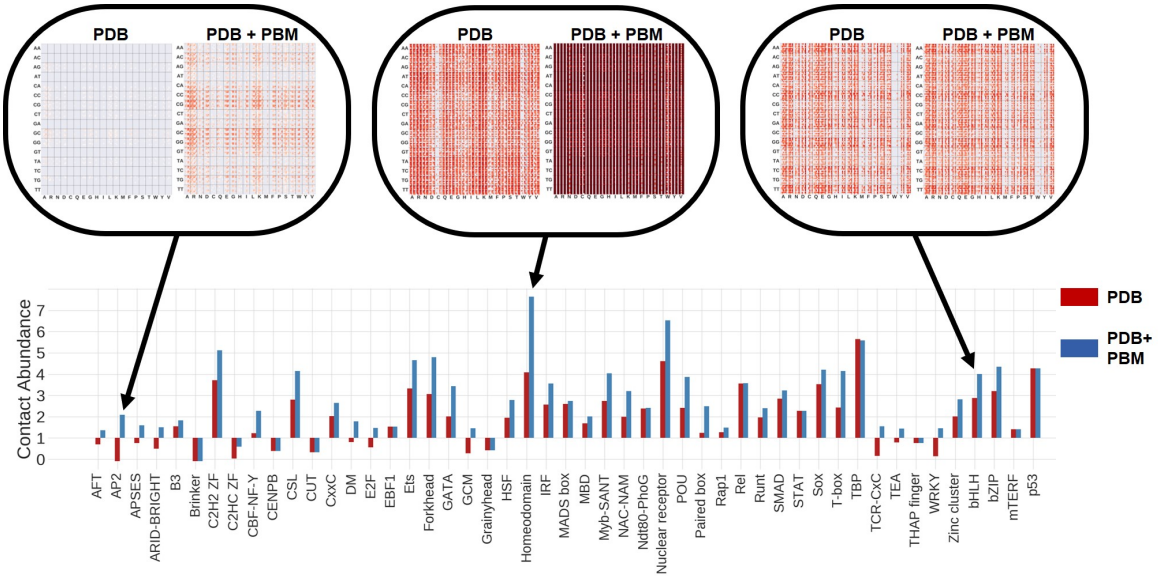

Figure 1: We defined the contact abundance score to capture the increase of coverage in the number and diversity of contacts thanks to the use of PBM experiments. This is defined as the logarithm of the ratio between the total number of potential accessible contacts and the number of contacts at less than 30Å. For the interaction between an amino-acid and two nucleotides there are 48 different types of contacts (considering the combination of all features, see supplementary methods), therefore the total number of potential contacts is 15360 (i.e. 4^2 x 20 x 48), while the number of real contacts depends on the number and quality of known structures of a TF family and in the PBM experiments that can be used to increase them. The figure shows the contact abundance score of each family calculated using only the known structures (PDB [42]) or including the potential (modelled) contacts of other TFs derived from PBM experiments (PDB+PBM). The figure shows in the top the heatmaps of the distribution of contacts, calculated with and without experimental PBM data, for three types of families (AP2, for which the use of PBM significantly increases the coverage; bHLH, for which the increase is not relevant; and the homeodomain family for which the coverage was already very large with only data from PDB). The labels and details of the heatmaps are shown as example in Figure S1. All heatmaps can be downloaded from http://aleph.upf.edu/modcre/##faq.

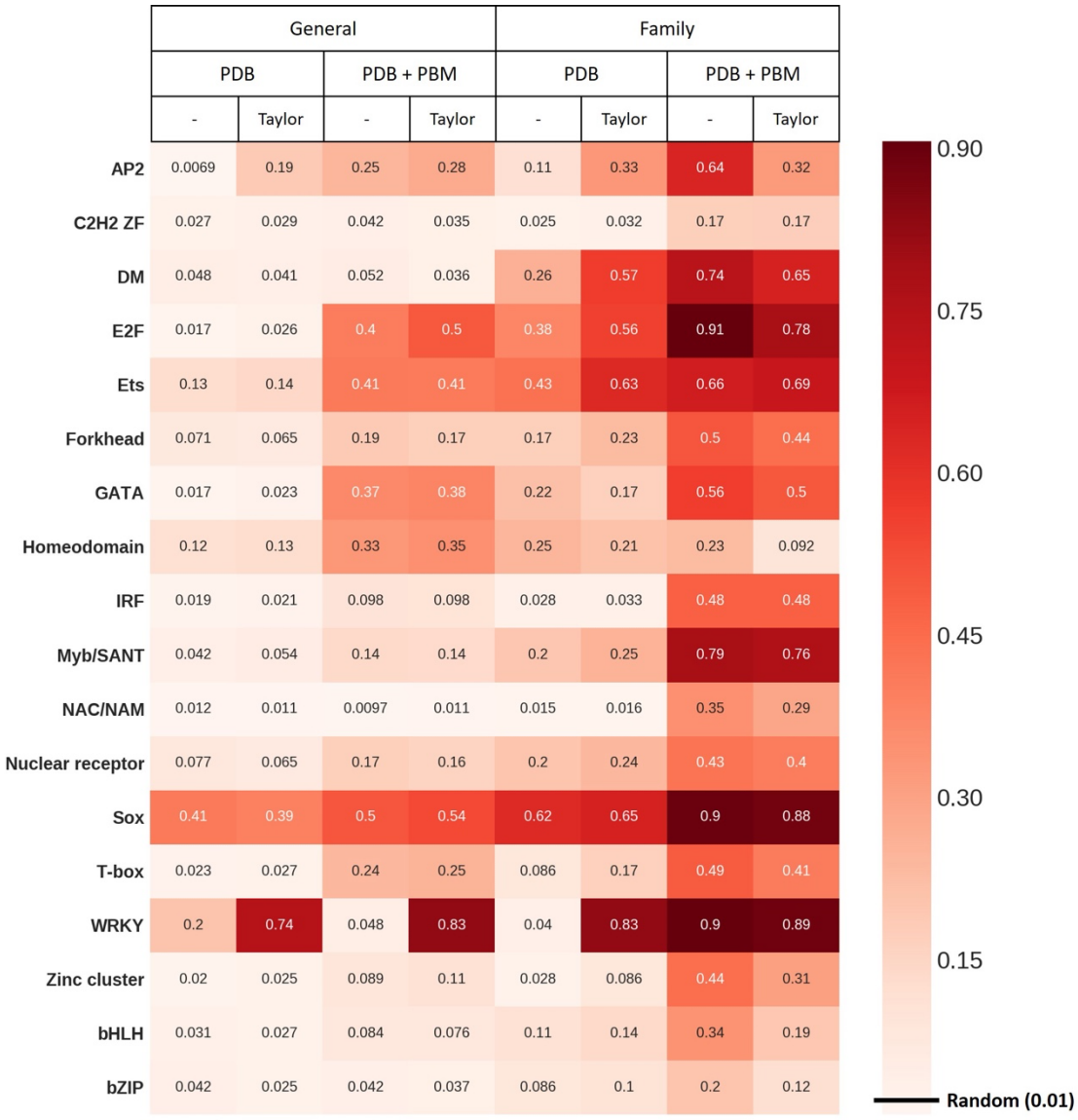

Figure 2

Area under the curve of precision-recall on the prediction of positive and negative 8-mers of the PBM experiments. We analyzed TFs of all families from Cis-BP database with PBM experiments. We used the PWMs predicted with the modelled structures of TFs, applying different structure-based features, to learn the best predictive model per family (i.e. using contacts extracted from PDB or from PDB plus those derived from PBM experiments, using only contacts obtained with TFs of the same family or contacts from all TFs -general-, or using a Taylor polynomial approach to complement the missing contacts in the experimental data). Not all negative 8-mers were used, forcing the balance ratio of positive/negatives to be 1 to 100 (negative 8-mers were selected randomly). We restricted the study to those families with at least

10 different TFs to sufficiently support the results (the test of the rest of families is in supplementary figure S2).

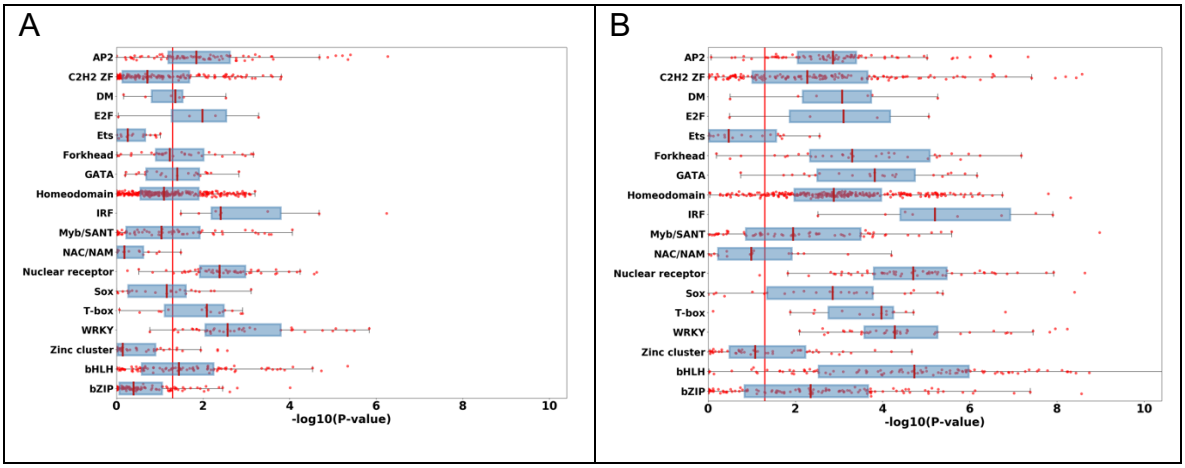

Figure 3.
Distribution of "similarity scores" to compare predicted and experimental PWMs of TFs. The score of similarity is defined as $-log_{10}(Pvalue)$, where the Pvalue is obtained with TOMTOM and it shows if the alignment of the two PWMs is significant (i.e. Pvalue is the probability that a random motif of the same width as the experimental PWM would have an optimal alignment as good or better than the PWM predicted with the structure of the TF). Each red dot in the plot shows either the average of scores (in A) or the highest score (in B) of the comparison of 100 predicted PWMs obtained with the structural models of each TF. Boxes in blue show the best quartiles of the distribution for each TF highlighting in red the mean of the distribution for all TFs of a family. A red line indicates the threshold at which the predicted PWMs are significatively similar to the experimental (i.e. Pvalue<0.05). For TFs of the C2H2-ZF family we used the parameters derived from a previous work[37]. As in Figure 2, we restricted the study to those families with at least 10 different TF sequences (the comparison with the rest of families of TFs is in supplementary figure S3).

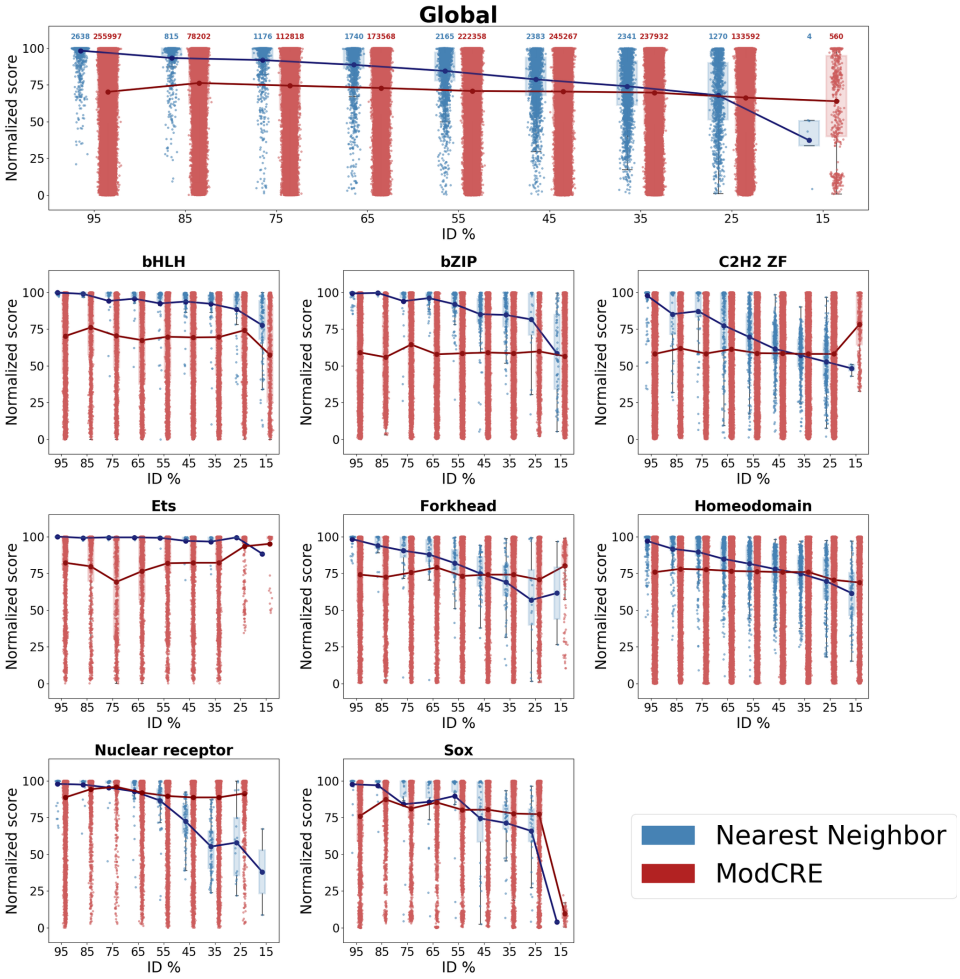

Figure 4

Distribution of the normalized ranking score of motif predictions with the nearest-neighbor (state-of-the-art) approach and the structure-based approach (ModCRE). Results with the nearest-neighbor approach are shown in blue and results with the structure-based approach in red. The top distribution (entitled Global) corresponds to the distributions for all TFs (i.e. 2638) in the dataset of CisBP with PBM experiments. The rank of the correct motif was scored and normalized with respect to the total size of the database of PWMs, yielding a normalized score. The normalized score is defined as: $normal\ score = 100 \times (2638 - rank + 1)/2638$. *The normalized score is null if the Pvalue of the comparison between the predicted PWM and the actual motif is higher than 0.05 (i.e. non-significative). At the top of the bins of the Global distribution are shown the total number of predicted motifs in each bin. The distributions of normalized scores of some families of TFs are also plotted (the title of each plot indicates the name of the family). Plots of distributions of normalized scores for the rest of families can be downloaded from the ModCRE webserver (http://aleph.upf.edu/modcre/##faq)*

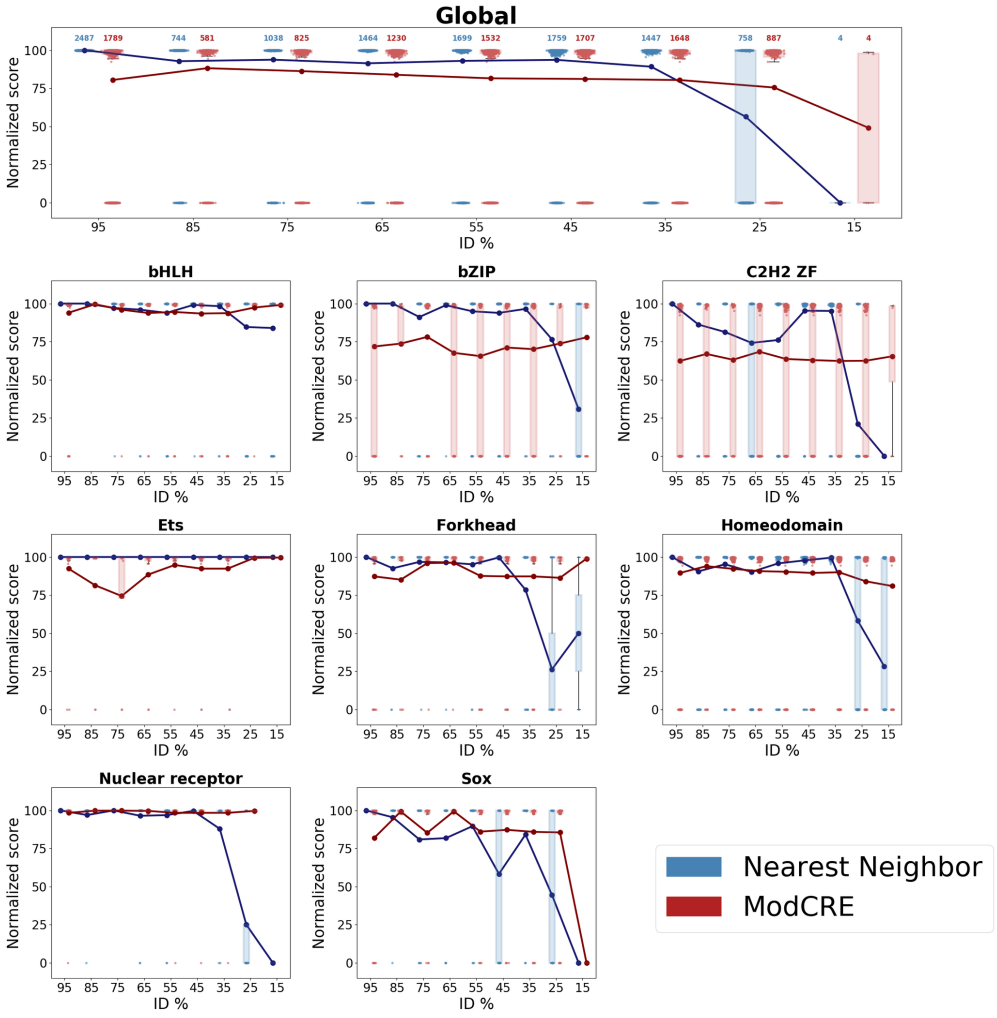

Figure 5
Distribution of the normalized ranking score of motif predictions with the nearest-neighbor (state-of-the-art) approach and the structure-based approach (ModCRE) using rank-enrichment. Results with the nearest-neighbor approach are shown in blue and results with the structure-based approach in red. Distribution titles and the normalized score are defined as in Figure 4. At the top of the bins of the Global distribution are shown the total number of predicted motifs in each bin. The distributions of normalized scores of the same families of TFs as in Figure 4 are also plotted.

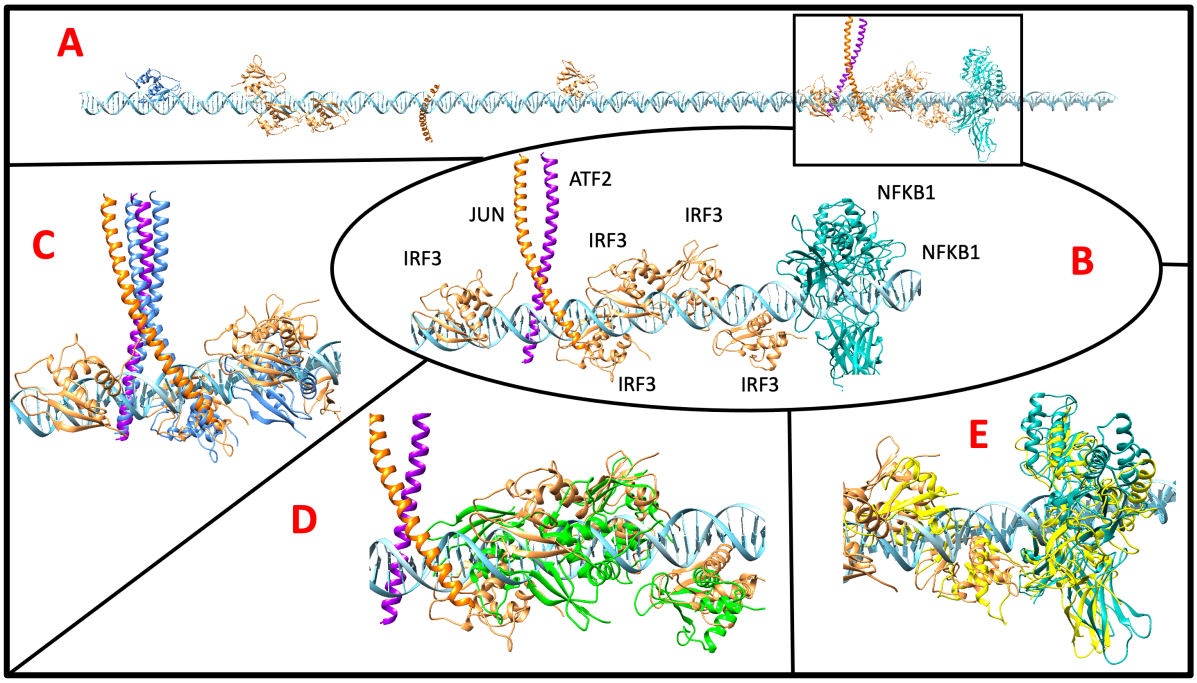

Figure 6

Model of the IFN-β enhanceosome complex. The structure of the complex formed by interactions between proteins and DNA is automatically built with the selected TFs and their binding sites in the enhancer sequence of IFN-β (see supplementary figure S4). A) Model of one of the complex structures obtained with the largest number of TFs while avoiding clashes between them. Due to the large time of computation, not all combinations of distinct conformations, produced by different templates, are tested. The structures of ATF-2 (purple), c-JUN (orange), IRF-3 (yeast) and NFKβ-1 (light blue) are shown on their binding with DNA (cyan), highlighting in a squared framework the region corresponding to the model of the enhanceosome proposed by Panne[21, 54]. B) Detail of the automated model obtained with ModCRE (IRF-3 is indicated as IRF3, ATF-2 as ATF2, c-JUN as JUN and NFKβ-1 subunit p105 as NFKB1): i) IRF-7 is missing; ii) NFKβ-1 forms a homodimer of two p105 subunits instead of the expected heterodimer with subunit p65 (RelA); and iii) an extra IRF-3 is bound at 5' of the ATF-2/c-Jun binding. C) Detail of the superimposition of the model of ModCRE with the crystal structure of ATF-2/c-Jun and IRF-3 bound to the interferon-beta enhancer (code 1T2K[60] from PDB, shown in blue). D) Detail of the superimposition of the model with the crystal structure of IRF-3 bound to the PRDIII-I regulatory element of the human IFN-β enhancer (code 2PI0[69] of PDB, shown in green). E) Detail of the superimposition of the automated model with the crystal structure of NFKβ-1 (subunits p105 and p65), IRF-7, and IRF-3 bound to the IFN-β enhancer (code 2O61[54] of PDB, shown in yellow).

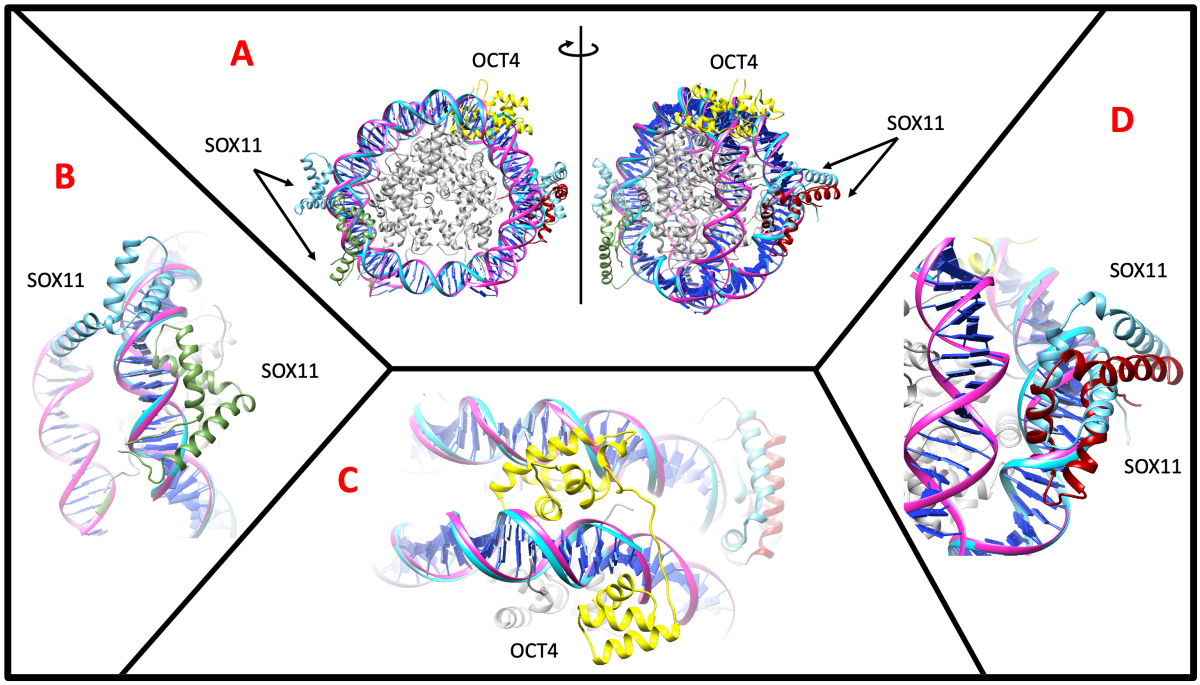

Figure 7
Model of the nucleosome complex with Sox11/Sox2 and Oct4. A) Front (left) and lateral (right) view of the complex obtained automatically with ModCRE superposed with the experimental structure (code 6T7C in PDB). Both model and experimental structures have only Sox11 bound (indicated as SOX11) to the nucleosome. The conformations modelled with ModCRE are shown in green (binding between 54 and 64 bps) and dark red (binding in the interval 86-96bps); the conformations of Sox11 from the experimental structure are shown in blue (binding in the interval of 50-60bps and 86-96 bps, respectively); and the model of Oct4 (indicated as OCT4) is shown in yellow (binding along an interval of 23-35bps). B) Detailed comparison of the binding of Sox11 between the automated model (green) and the experimental structure (blue). The predicted PWM fails to position neither Sox11 nor Sox2 around the 50bp (the closest fragment is in the interval of 54-57bps). C) Detail of the modelled binding of Oct4 (in yellow). Two domains of Oct4 produce the binding in a large interval of the DNA sequence (between 23 and 35bps), where the domain that binds in 3' (around 28-35 bps) has also "non-binding" contacts (with many clashes) with the DNA fragment around 98-112bps. This suggests a potential weakening of the nucleosome complex conformation that could lead to unfasten it. D) Similar binding of Sox11 around 86-96bps of the model (dark red) and experimental (blue) structures. The DNA sequence used in the model is DNA1 from the study of Dodonova et al.[22] *:*
ATCTACACGACGCTCTTCCGATCTAATTTATGTTTGTTAGCGTTATACTATTCT
AATTCTTTGTTTCGGTGGTATTGTTTATTTTGTTCCTTTGTGCGTTCAGCTTAAT
GCCTAACGACACTCGGAGATCGGAAGAGCACACGTGAT

Tables

Table 1

Logos of experimental PWMs (from JASPAR and CisBP) and of their best predictions. The table shows the logos of only some TFs for which the PWMs were also obtained by PBMs in CisBP. The TF is identified by the UniProt code. The code of the PWMs corresponding to the logos in JASPAR and CisBP are shown at the bottom. For the logos of the predicted PWMs the PDB code of the protein used as template is shown at the bottom. The logos of TFs from other families is shown in supplementary Table S1.

Uniprot	Family	JASPAR	CisBP	ModCRE
Q9SFE4	AP2	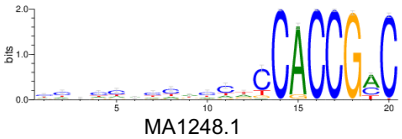 MA1248.1	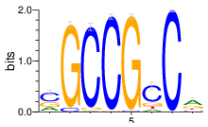 M01615	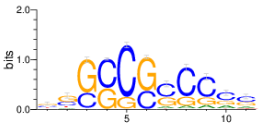 1gcc
P61244	bHLH	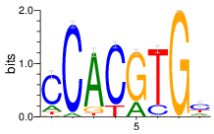 MA0058.3	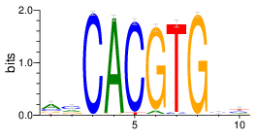 M00938	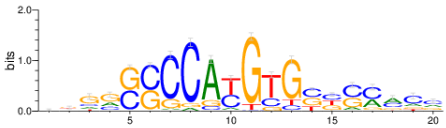 1an4
Q9NP62	GATA	 MA0766.1	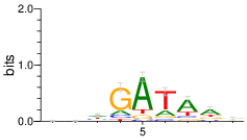 M00167	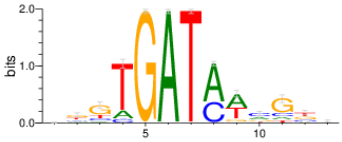 4gat
P10276	Nuclear receptor	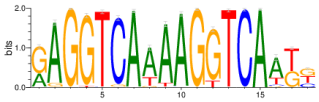 MA0729.1	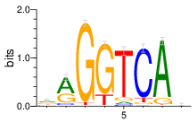 M00185	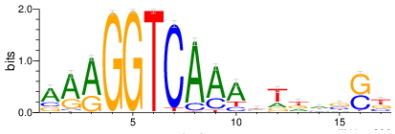 1r0n
O15119	T-box	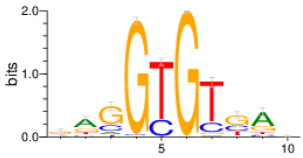 MA1566.1	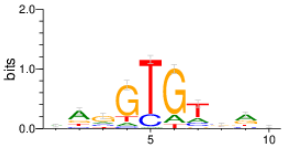 M00834	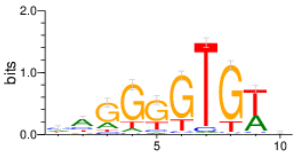 2x6v
Q8VWJ2	WRKY	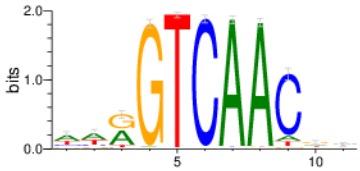 MA1311.2	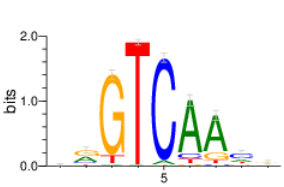 M02564	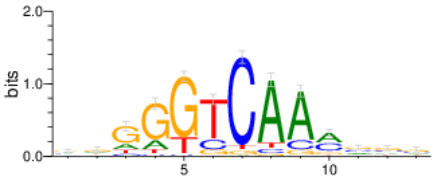 6ir8

Supplementary Figures

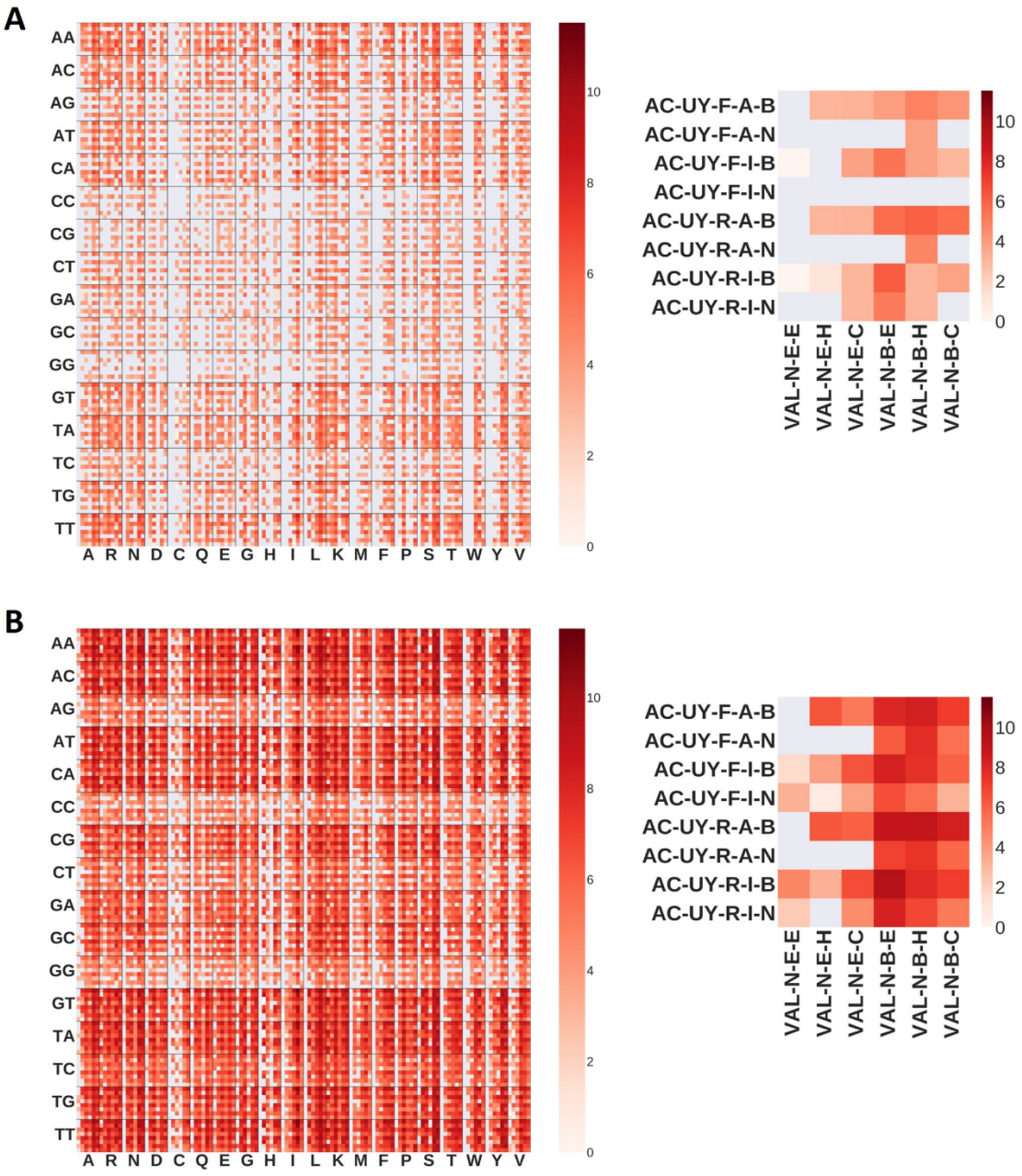

Figure S1. Examples of heatmap plots showing the number of amino acid—dinucleotide contacts at distance shorter than 30Å in a logarithmic scale. (A) Example of amino-acid and dinucleotide contacts extracted from PDB structures of the Forkhead family. (B) Example of amino-acid and dinucleotide contacts obtained from PDB structures and PBM experiments of transcription factors of the Forkhead family. Detailed view of a cell in each heatmap is shown in the right side. Each square inside the cell shows the logarithm of the number of contacts with specific

features. The example shows the contacts between a valine amino-acid (VAL) and a dinucleotide of adenosine-cytosine (AC), with their specific environment features. Amino-acid environment features are: hydrophobicity (P as polar, N non polar), surface accessibility (E if exposed, B if buried) and secondary structure (E for β-strand, H for helix and C for coil). Dinucleotide "environment" features are: type of nitrogenous bases (U for purine, I for pyrimidine), closest DNA strand (F for forward, R for reverse), closest DNA groove (A for major, I for minor) and closest chemical group (B if phospho-ribose backbone atoms, N if nucleobase). All heatmaps can be downloaded from the web in http://aleph.upf.edu/modcre/##faq.

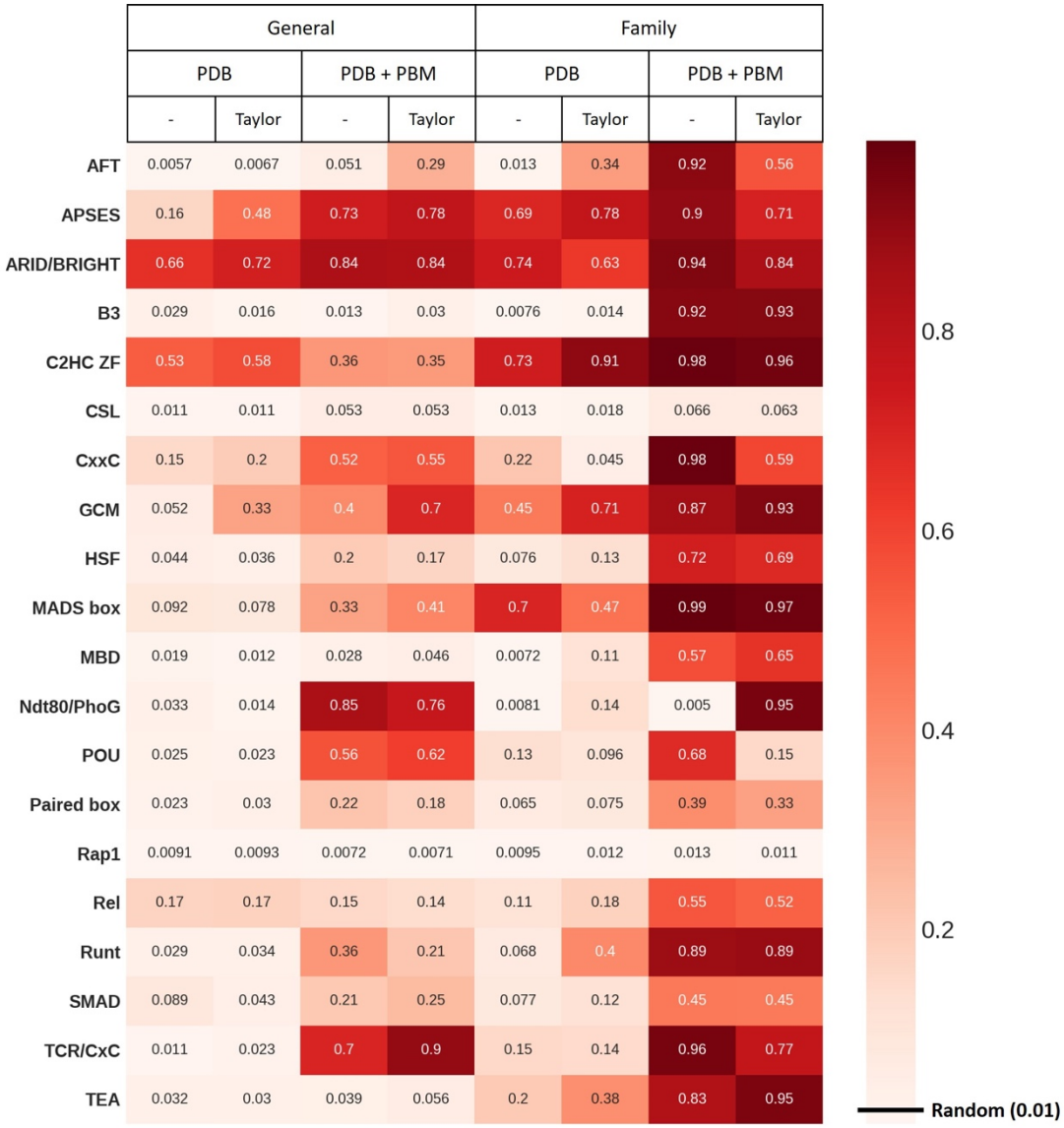

Figure S2

Area under the curve of precision-recall on the prediction of positive and negative 8-mers of the PBM experiments. We analyzed TFs of all families from Cis-BP database with PBM experiments. We used the PWMs predicted with structural models of TFs using different features to calculate the ZES3DC$_{dd}$ score (such as the use of the Taylor polynomial approach, using contacts extracted from PDB or from PDB plus those derived from PBM experiments or using only contacts obtained with TFs of the same family). Not all negative 8-mers were used, forcing the ratio of positive/negatives to be 1 to 100 (negative 8-mers were selected randomly). The table shows the study of families with less than 10 different TFs supporting the results

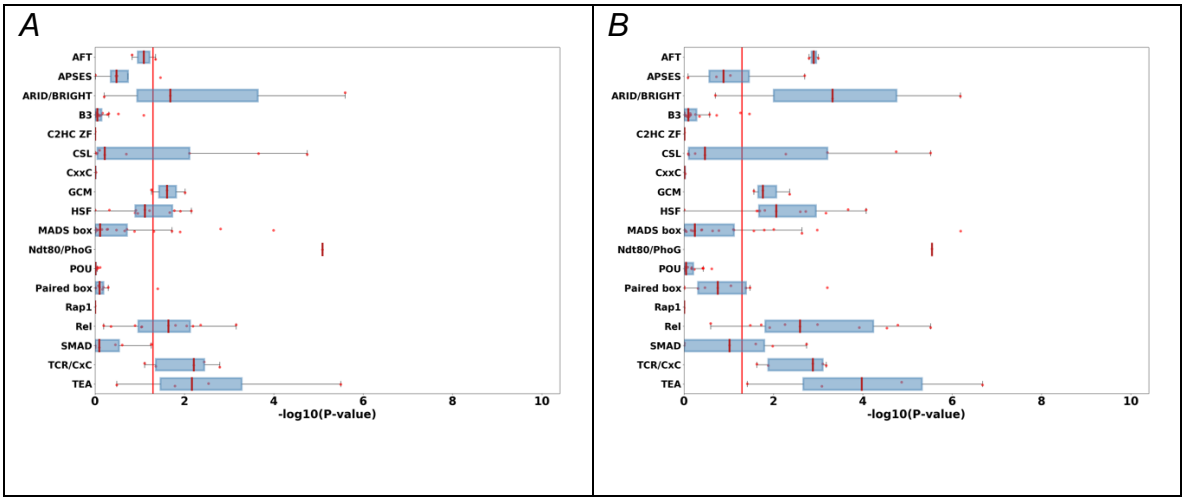

Figure S3
Distribution of "similarity scores" to compare predicted and experimental PWMs of TFs. Legends are as in Figure 3. Plots correspond to TF families with less than 10 different TF sequences.

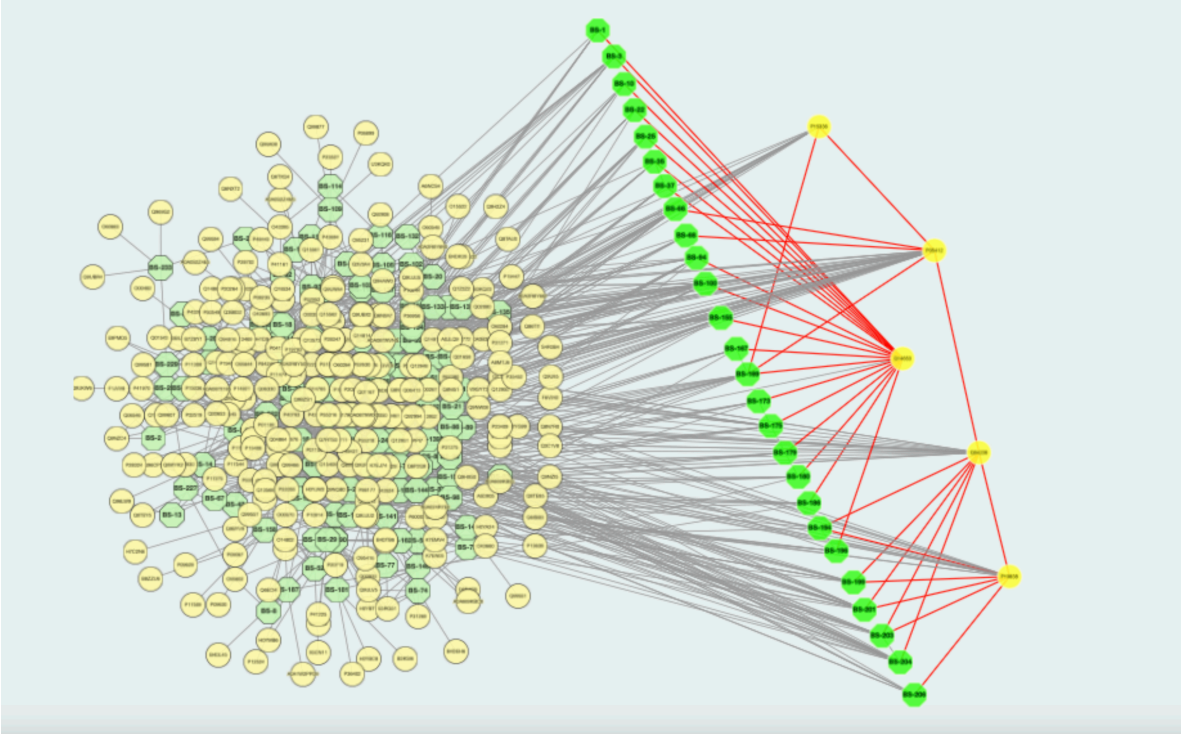

Figure S4

Cis-regulatory elements of the IFN-β enhancer site and its potential transcription factors. Selected bindings of c-Jun (P05412), ATF-2(P15336), IRF-3(Q14653), IRF-7(Q92985), NFKβ-1 subunit p105 (P19838) and RelA(Q04206) human transcription factors on the enhancer region of the IFN-β (formed by 250 bps). Uniprot codes of these proteins are shown within parenthesis. Bindings are selected with a significant match (P-value < $5.0e^{-4}$) of the PWM predicted with the structure using ModCRE and achieving the top scores (i.e. normalized $ZES3DC_{dd}$ values, see supplementary material). Under these conditions IRF-7 is not selected and a molecule of IRF-3 occupies its location. Transcription factors are shown in yellow and binding sites in green. Interactions between TFs and between TFs and binding sites are shown as edges. Edges between the selected TFs and their binding sites are shown in red. The rest of interactions (in black) correspond to interactions of these TFs with other human proteins (also TFs). The sequence of the enhancer region of IFN-β is GTTTGCTTTCCTTTGCTTTCTCCCAAGTCTTGTTTTACAATTTGCTTTAGTCATT CACTGAAACTTTAAAAAACATTAGAAAACCTCACAGTTTGTAAATCTTTTTCCCT ATTATATATATCATAAGATAGGAGCTTAAATAAAGAGTTTTAGAAACTACTAAAA TGTAAATGACATAGGAAAACTGAAAGGGAGAAGTGAAAGTGGGAAATTCCTCT GAATAGAGAGAGGACCATCTCATATAAATAGG.

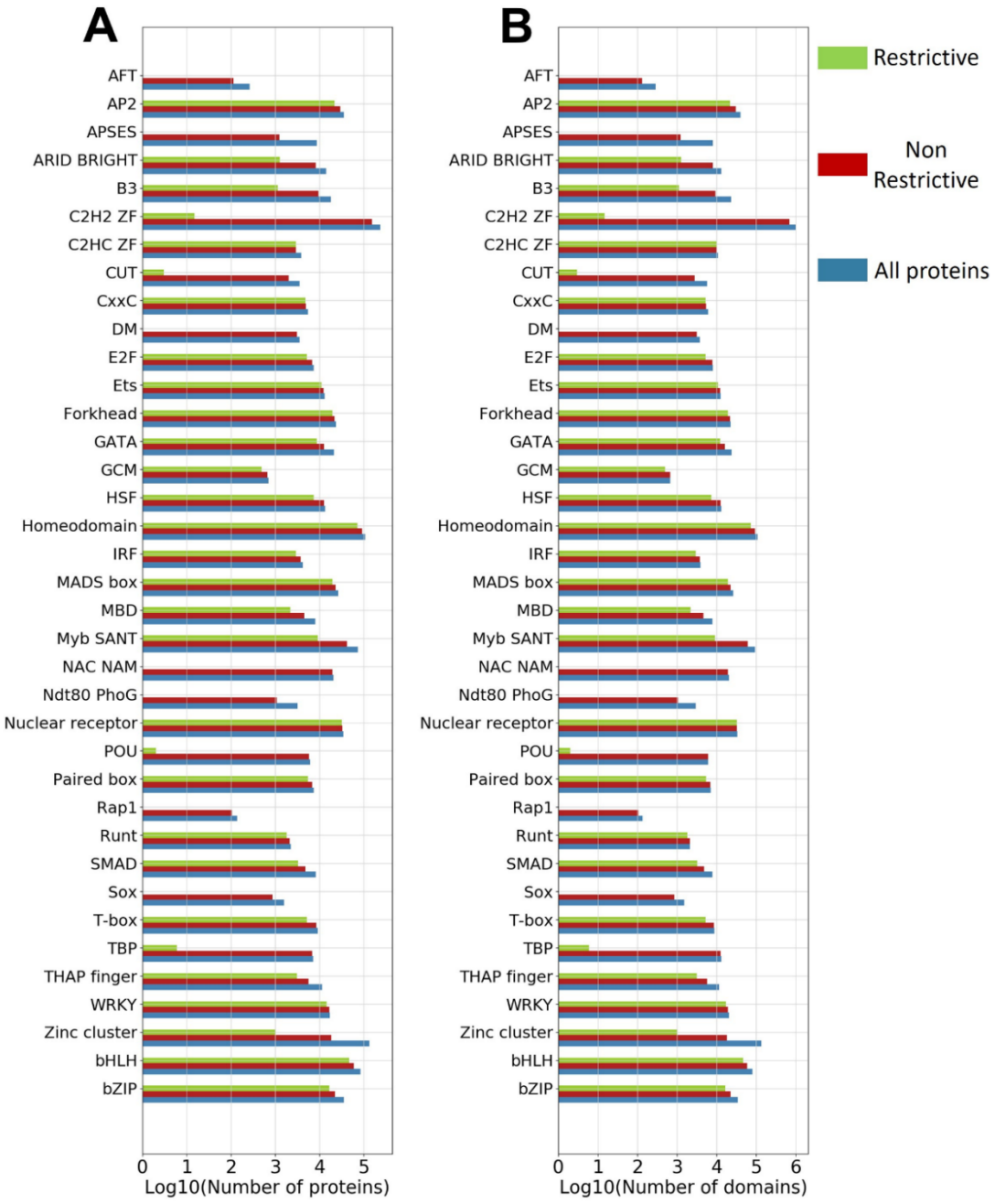

Figure S5

Applicability of the structure-based approach to predict TF motifs using homology modelling. The plots show the total number of proteins (A) and domains (B) for which a PWM can be predicted using homology modelling (applying the server of ModCRE). TF families are indicated in the vertical axis versus the logarithm of the number of proteins (or domains), showing: i) the total number of UniProt sequences

that match the PFAM model of the family (blue); ii) those that can be modelled without gaps in the interface of the interaction with DNA (green); and iii) and those with gaps in the interface (red).

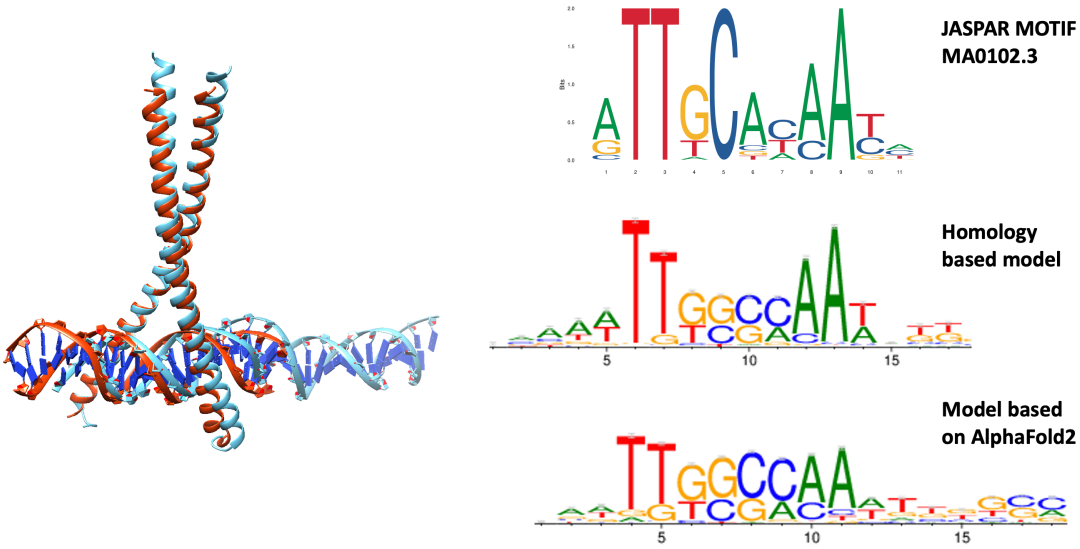

Figure S6

Prediction of PWMs of human C/EBPα. The ribbon plate structures on the left side show the superposition of a model of human C/EBPα (red) obtained with the crystal structure of rat (code 1NWQ in PDB) as template and a model based on the structure predicted with AlphaFold2 (blue). The right side shows a comparison of the motif logos of human C/EBPα: i) the top logo corresponds to motif MA0102.3 from JASPAR; ii) the middle logo is obtained with the prediction based on the homology model of human C/EBPα; and iii) the bottom logo is obtained with the structure modelled upon the structure prediction of human C/EBPα obtained with AlphaFold.

Supplementary Tables

Table S1
Logos of experimental PWMs (from JASPAR and CisBP) and of their best predictions. The table shows the logos of one TF per family, selected from Table S2, with a good match with at least one of the experimental PWMs. We only used TFs for which the PWMs were also obtained by PBMs in CisBP as in Table 1. Labels are as in Table 1.

Table S2
Summary of the analysis of predicted PWMs of TFs with experimental motifs in JASPAR and CisBP (obtained with PBM). The ID code of the TF as defined in CisBP is shown in the first column (TFID). Second and third columns show the name of the family (also as coded in CisBP). Fourth and fifth columns show the UniProt code of the TF and the encoded name of the model used to generate the PWM most similar to the motif in JASPAR. The code of the model identifies the TF, the first and last amino acids of the modelled sequence, the PDB code of the template and the chain, and a number to identify the model out of 100. Sixth and seventh columns show the codes of the motifs in JASPAR and CisBP datasets, respectively. Eight and nineth columns show the ratio of models yielding PWMs that significatively align with the experimental motif of JASPAR and CisBP, respectively. Successes are identified in the last four columns with a Boolean (1 if right, 0 if wrong). In the first two columns of the last four we define the success by the ratio (if more than 50% of predicted PWMs were significatively aligned with the experimental motif) for the JASPAR and CisBP motifs, respectively. In the last two columns we define the success if at least one of the predicted PWMs aligned significatively with the experimental motif from JASPAR and CisBP, respectively.